RSC Advances

PAPER

View Article Online
View Journal | View Issue

Cite this: *RSC Adv.*, 2024, **14**, 9975

Surface ligand modified silver nanoparticles-based SERS sensing platform for ultrasensitive detection of the pesticide thiram in green tea leaves: roles of coating agents in sensing performance†

Dong Thi Linh,[ab] Quan-Doan Mai, *[a] Dao Thi Nguyet Nga,[a] Nguyen Tuan Anh,[a] Hoang Van Tuan,[a] Ha Anh Nguyen, *[a] Xuan Hoa Vu[c] and Anh-Tuan Le *[ad]

Silver nanoparticles (AgNPs) have been regarded as a highly promising substrate for surface-enhanced Raman scattering (SERS) sensors. In this study, we focused on the electrochemical synthesis method by developing three kinds of AgNPs using three different electrolytes: citrate (e-Ag-C), oleic acid (e-Ag-O) and fish mint (*Houttuynia cordata* Thunb.) extract (e-Ag-bio). The as-prepared AgNPs were characterized and then employed as SERS substrates to detect the pesticide thiram. The obtained results show that e-Ag-O exhibits the best SERS performance. The effect of the coating agent was explained by chemical and electromagnetic enhancements (CM and EM). Although thiram could absorb onto e-Ag-C at the highest level, allowing its Raman signal to be best enhanced *via* the CM, the smallest interparticle distance of e-Ag-O could have resulted in the largest improvement in the EM. Using e-Ag-O to develop SERS-based sensors for thiram, we obtain the impressive detection limit of 1.04×10^{-10} M in standard samples and 10^{-9} M in tea leaves. The linear ranges are from 10^{-4} M to 10^{-7} M and from 10^{-7} M to 10^{-9} M, covering the maximum residue levels for plant commodities established by the United States Environment Protection Agency and European Food Safety Authority (2–13 ppm ~7.7×10^{-6} M to 5×10^{-5} M).

Received 3rd January 2024
Accepted 20th March 2024

DOI: 10.1039/d4ra00048j

rsc.li/rsc-advances

1. Introduction

Surface-enhanced Raman spectroscopy (SERS) is a powerful analytical tool, which can detect numerous organic compounds at trace levels based on their unique vibrational fingerprinting.[1,2] The enhancement of the Raman signal of analytes requires their adsorption onto a SERS-active substrate, which could generate a localized surface plasmon resonance (LSPR) phenomenon. It occurs due to oscillation of electrons on the surface of the substrate excited by a laser source, leading to the formation of a strong electromagnetic field around their surface.[3] As a result, the Raman signal is significantly enhanced in the electromagnetic mechanism (EM).[3] It was reported that EM enhancements are elevated within specific regions with intense electromagnetic fields, called hotspots, including the sharp tips and corners of NPs, as well as the small gaps (<10 nm) between them.[3–5] On the other hand, the adsorption of the analyte on the surface of the NPs promotes substrate-to-molecule charge transfer (CT). It would change electron density distribution within the analyte, therefore, creating notable polarization and then causing Raman scattering. This enhancing mechanism is regarded as the chemical mechanism (CM).[3]

As LSPR is the key for the generation of the SERS phenomenon, noble metal nanoparticles (NP) with strong plasmonic resonances, such as Au and Ag, have been employed as promising SERS substrates.[6,7] While Au-based NPs have been regarded as the best plasmonic materials for biosensors thanks to their biocompatibility and low toxicity, Ag-based NPs exhibit stronger plasmonic resonances and better cost-effectiveness, allowing fabrication of sensitive chemosensors for chemical compounds. While it is known that AgNPs are significantly less robust and more susceptible to air than AuNPs, these issues can be solved by using different types of both reducing and capping agents to inhibit the oxidative process. Many kinds of AgNPs

[a]*Phenikaa University Nano Institute (PHENA), Phenikaa University, Hanoi 12116, Vietnam. E-mail: doan.maiquan@phenikaa-uni.edu.vn; anh.nguyenha@phenikaa-uni.edu.vn; tuan.leanh@phenikaa-uni.edu.vn*

[b]*Faculty of Fundamental Sciences, Thai Nguyen University of Technology, 666 3/2 Road, Thai Nguyen City 24000, Vietnam*

[c]*Institute of Science and Technology, TNU-University of Sciences, Tan Thinh Ward, Thai Nguyen City 24000, Vietnam*

[d]*Faculty of Materials Science and Engineering (MSE), Phenikaa University, Hanoi 12116, Vietnam*

† Electronic supplementary information (ESI) available. See DOI: https://doi.org/10.1039/d4ra00048j

have been designed and developed as SERS substrates, using physical and chemical synthesis methods.[8–11] For example, Singh's group has fabricated Ag zigzag and Ag nanorod arrays using a glancing angle deposition technique to promote EM enhancement of SERS signal.[10,12] However, the physical synthesis of AgNPs requires extreme conditions and expensive equipment. On the other hand, AgNPs have been generated thanks to the reduction of Ag salts in chemical approaches. Different reducing agents such as ethylene glycol, polyethylene glycol and citrate have been employed to fabricate AgNPs in various studies.[13–15] Among them, acting as both a reducing agent and a capping agent, citrate has been widely used. Citrate-coated AgNPs have been employed to develop numerous SERS-based sensors.[11,15,16] In addition, a green approach of AgNP synthesis has been proposed with the use of plant extracts. Santos *et al.* fabricated AgNPs self-assembled on glass substrates using three citrus peel extracts, including orange, tangerine and lemon and employed lemon extract-prepared AgNPs as SERS substrates for detection of 4-amino-benzenethiol, rhodamine 6G and methylene blue.[17] Recently, electrochemically synthesized AgNPs (e-AgNPs) have shown their potential as SERS substrates. The fabrication procedure only requires two silver electrodes and an electrolyte in water, which acts as both a reducing agent and a capping agent. Therefore, it reduces the use of chemicals, leading to high purity of prepared AgNPs, onto which analytes can effectively adsorb and experience a significant enhancement of SERS signal.[18] Many kinds of AgNPs have been fabricated using different reducing and capping agents for SERS applications. Nevertheless, there has been no study investigating the effect of those agents on SERS sensing performance, especially for e-AgNPs.

To fill in the gap, in this study, we synthesized three kinds of e-AgNPs using different types of electrolyte substance: citrate (e-Ag-C), oleic acid (e-Ag-O), and fish mint (*Houttuynia cordata* Thunb.) extract (e-Ag-bio). Their SERS sensing performance was investigated and compared using thiram, a widely-used pesticide, as an analyte, resulting in the best performance of e-Ag-O The difference in SERS effect on those e-AgNPs was explained in terms of CM and EM. As the most suitable SERS substrate, e-Ag-O was then employed to develop SERS sensors for thiram with detection limit (LOD) of 1.04×10^{-10} M and quantification range of 10^{-4} M to 10^{-7} M and 10^{-7} M to 10^{-9} M. In real samples of tea leaves, the e-Ag-O-based sensors could determine the presence of thiram at concentrations down to 10^{-9} M.

2. Material and methods

2.1. Material and SERS substrates

Sodium citrate ($Na_3C_6H_5O_7$, 99.9%), oleic acid ($C_{18}H_{34}O_2$, 99%) and thiram ($C_6H_{12}N_2S_4$, 97.0%) were purchased from Sigma Aldrich and used directly without further purification. Two silver plates (purity: 99.99%) were prepared with dimensions of (100 mm × 5 mm × 0.5 mm).

Fish mint was purchased from a local market in Vietnam, washed properly with water, and dried naturally under shade. Subsequently, they were cut into fine pieces. 100 g of dry fish mint was then immersed into 300 mL of distilled water at room temperature (RT). The mixture was incubated at 70 °C for 60 min upon constant stirring. Finally, 20 mL of fish mint extract was obtained. It was then diluted to reach the volume of 200 mL using distilled water for the following experiments.

Aluminum (Al) substrates were fabricated as described in our previous study with dimensions of 1 cm × 1 cm × 0.2 cm with a surface-active area with a diameter of 0.2 cm.[18] The substrates were immersed into a diluted hydrochloric acid solution and washed with ethanol and double distilled water by ultrasonication for 15 min, followed by being dried properly at RT.

2.2 Synthesis and characterization of e-Ag-C, e-Ag-O and e-Ag-bio

e-AgNPs were synthesized using an electrochemical method, which was described in our previous study with several modifications.[18] A two-electrode setup was prepared as described in Scheme 1. The electrochemical syntheses of three kinds of e-AgNPs were taken place in a beaker containing 200 mL of electrolyte solution. To prepare different e-AgNPs, electrolyte solutions were different. To be detailed, $Na_3C_6H_5O_7$ and $C_{18}H_{34}O_2$ solutions at the same concentration of 6×10^{-5} M were employed to fabricate e-Ag-C and e-Ag-O, respectively. The prepared fish mint extract was used to generate e-Ag-bio. Electrochemical syntheses were carried out at RT under uniform magnetic stirring at 200 rpm for 60 min, under electrolytic of 12 V. The morphology of as-prepared e-AgNPs was investigated using scanning electron microscopy (SEM, Hitachi S-4800) operated at an acceleration voltage of 5 kV. Their ultraviolet-visible (UV-vis) absorption spectra were recorded using a JENWAY 6850 double-beam spectrophotometer using 10 mm-pathlength quartz cuvettes. Powder X-ray diffraction (XRD, BrukerD5005 X-ray diffractometer) with strictly monochromatized Cu Kα ($\lambda = 1.5406$ Å) under a voltage of 40 kV and a current of 30 mA was employed to identify the phase and chemical composition of the samples.

2.3. SERS measurements

To prepare SERS substrate, 20 μL of colloidal e-AgNP solution was drop-casted on the surface-active area of the Al substrate and dried at RT. Thiram solutions (10^{-4} M to 10^{-10} M) were prepared in distilled water. For each SERS measurement, 5 μL of thiram solution was drop-casted directly onto the prepared SERS substrate and dried naturally at RT. SERS spectra were recorded using a MacroRaman™ Raman spectrometer (Horiba) with a 100× objective with a numerical aperture of 0.90, at a focal length of 115 nm, using the laser power 45 mW at a 60° contact angle. An exposure time of 15 s was used with one accumulations.

Fresh tea leaves were purchased from a local market in Thai Nguyen province (Vietnam) and homogenized thoroughly. 300 mL of distilled water was added into 100 g of this mixture and mixed well using a vortex mixer, followed by 15 min of ultrasonication. The mixture was then filtered using Whatman filter paper to eliminate large and centrifugated to collect the

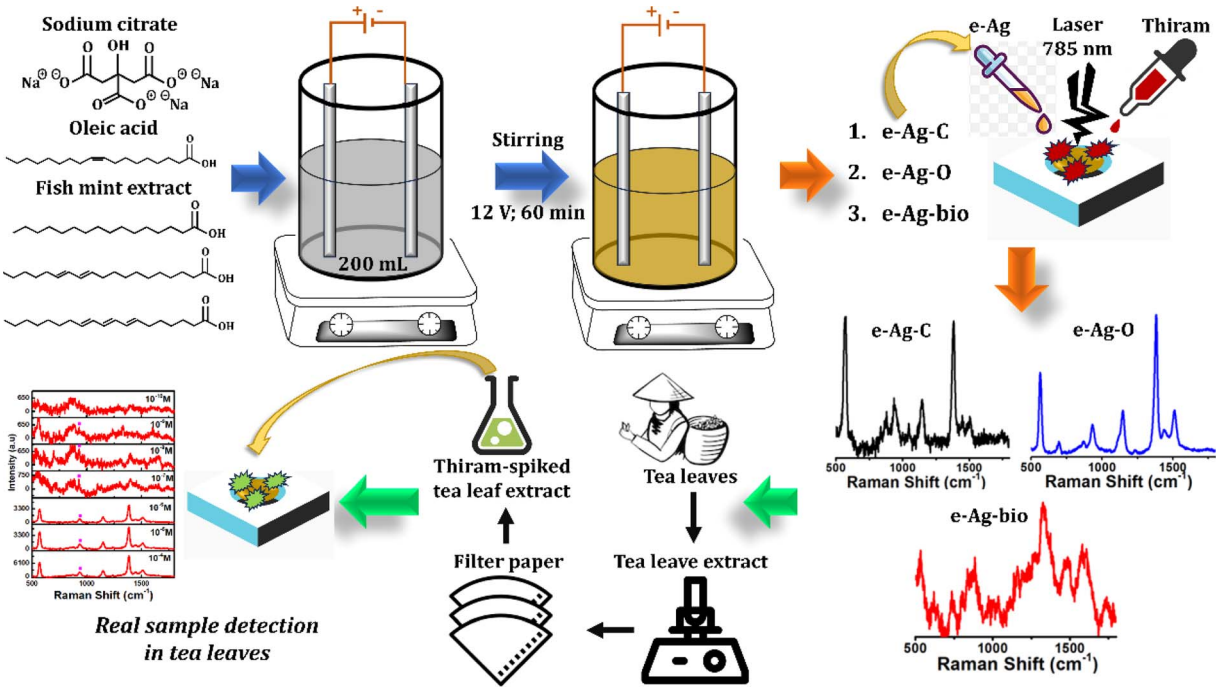

Scheme 1 Schematic illustration of the synthesis process of e-AgNPs.

supernatant. Thiram-spiked tea leaf extract was prepared by adding suitable volumes of thiram standard solutions into the extract. Similar to the standard samples, the spiked ones were then drop-casted onto the SERS substrates for SERS measurements.

3. Result and discussion

3.1. Characterization of e-Ag-C, e-Ag-O and e-Ag-bio

Fig. 1a shows absorption spectra of the colloidal e-Ag-C, e-Ag-O and e-Ag-bio, revealing SPR bands at 413 nm, 415 nm and 435 nm, which are characteristic of e-AgNPs. Accordingly, SPR peaks of e-Ag-C and e-Ag-O are only slightly different. Meanwhile, using fish mint exact as the electrolyte for e-AgNP synthesis resulted in a significant red-shift of around 20 nm in SPR band, compared to the use of the other electrolytes. Although the coating layer of e-Ag-bio was expected to be complex due to complicated components within the fish mint extract as listed in Scheme 1 and reflected in its absorption spectrum in Fig. 1a, such large red-shift might be also related to the difference in size of e-AgNPs fabricated using those different electrolytes or even the aggregation of e-Ag-bio. Nevertheless, there was no large aggregation of e-Ag-bio, which could be observed with bare eyes. A closer look was provided by SEM images. Concerning e-Ag-C, Fig. 1d reveals the formation of spherical e-AgNPs with sizes ranging from 15 nm to 30 nm with a particle size distribution histogram. The mean diameter of e-Ag-C was calculated to be 21 nm using the equation:

$$\overline{d} = \frac{\sum_{k=0}^{n} x_k f_k}{N} \quad (1)$$

in which d is the mean diameter, x_k is the diameter of the kth nanoparticle, f_k is the frequency of the kth diameter and N is the sum of the f_k ($k = 0,1,2\ldots n$). The mean hydrodynamic diameter (Z-average) of e-Ag-C sample was calculated to be 36.8 nm (Fig. S1b†), which was consistent with the SEM result.

Using oleic acid, spherical e-AgNPs were also fabricated with smaller sizes. Fig. 1c shows NPs with sizes ranging from 10 nm to 25 nm. The mean diameter of e-Ag-O from SEM and DLS measurements were estimated to be 16 and 22.8 nm, respectively (Fig. S1a†). Despite a smaller mean diameter, the SPR band of e-Ag-O is shifted 2 nm toward the longer wavelength compared to that of e-Ag-C. As no aggregation was observed either in solution nor on SEM images (Fig. 1c and d), the difference in coating molecule could be responsible for this minor shift. Concerning e-Ag-bio, the SEM image explains its large shift in its SPR band compared to the others. Fig. 1e demonstrates bright particles covered by a gel-like layer. The sizes of these particles range from 15 nm to 40 nm with a mean value of 26 nm, which is not much larger than that of e-Ag-C. Instead, several clumps of 5–10 NPs gathering could be observed in the SEM image. However, the SEM image shows that they are not completely aggregated but separated from each other by their coating layers. In another word, they have been agglomerated. The NP clumps were not large enough to be detected with bare eyes, however, it was reflected in absorption spectra with SPR band at 435 nm. This observation is consistent with the hydrodynamic diameter value of e-Ag-bio sample from DLS measurement (58.7 nm). In addition, the surface charge of Fig. S2† show that both e-Ag-C and e-Ag-bio are negatively charged with ζ potential values of −21.2 mV and −15.1 mV. Meanwhile, e-Ag-O is nearly neutral, leaning toward negative side with ζ potential of −5.8 mV. It could be due to the unique

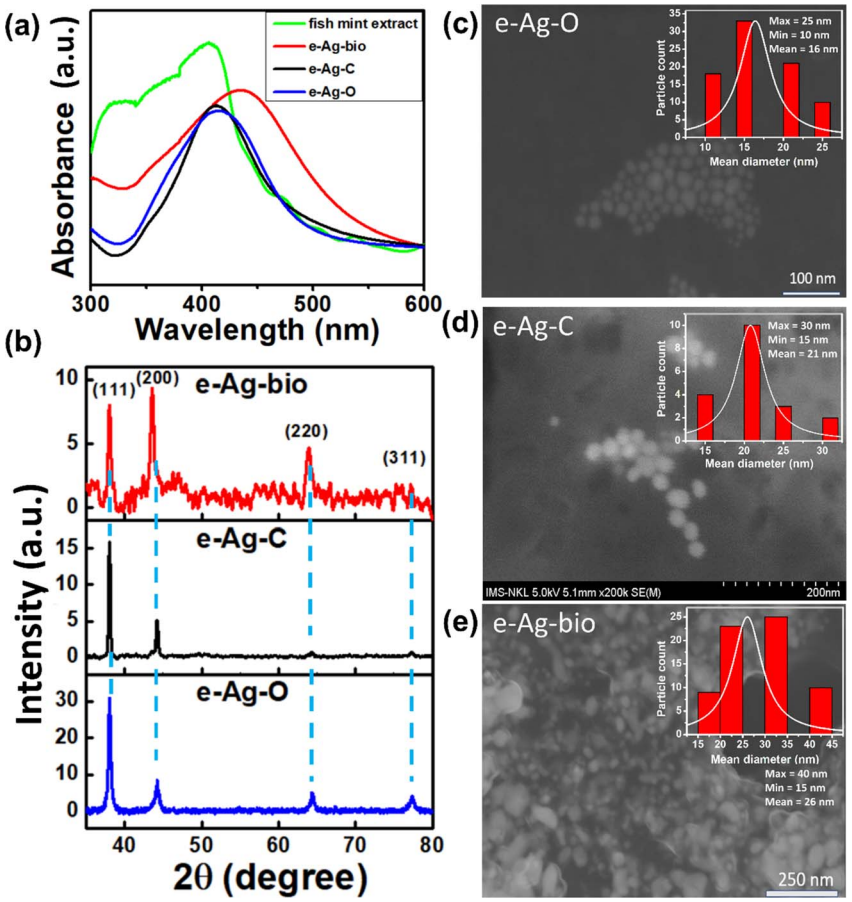

Fig. 1 (a) UV-vis spectra of fish mint extract, e-Ag-bio, e-Ag-C and e-Ag-O; (b) XRD patterns of e-Ag-O, e-Ag-C and e-Ag-bio; (c)–(e) SEM images of e-Ag-O, e-Ag-C and e-Ag-bio, respectively.

properties of oleic acid. Each oleic acid molecule consists of a hydrophilic head of carboxyl group and a hydrophobic hydrocarbon tail. After the formation of e-AgNPs, the carboxyl group was attached to the Ag surface. Therefore, if e-AgNPs were capped by only a monolayer of oleic acid, as-prepared e-Ag-O could be hydrophobic.[19] In this study, e-Ag-O, in contrast, is well dispensed in aqueous media. In a 2020 study, Khutsishvili *et al.* proposed the formation of a secondary layer thanks to C=C double bonds resulting from coupling of delocalized p-electrons between two layers, exposing carboxylic groups on the surface of AgNPs, allowing them to be dispensed in aqueous media.[19] This description is appropriate for the properties of e-Ag-O in this study. However, the formation of C=C double bonds between two layers has decreased electrostatic potential of the exposed carboxylic groups. Thus e-Ag-O is nearly neutral. As e-AgNPs coated with citrate are negatively charged, electrostatic repulsion would have separated them from each other in solution, leading to the increase in interparticle distance. Interestingly, the interparticle distance between e-Ag-C NPs is also larger than that between e-Ag-O NPs on SEM images. The average distances between e-Ag-C NPs and e-Ag-O NPs were estimated to be 7 nm and 4 nm, respectively. The pH values of e-Ag-O, e-Ag-C, and e-Ag-bio samples were also measured to be about 8.2, 8.7, and 5.2, respectively.

The crystallization of three kinds of e-AgNPs was investigated using X-ray diffraction (XRD). Fig. 1b shows their XRD patterns with peaks corresponding to metallic phase of Ag with the main diffraction peaks for the (111), (200), (220) and (311) crystalline planes, corresponding to JCPDS No. 00-004-0783. It is noticeable that the XRD pattern of e-Ag-O sample exhibits more diffraction peaks with higher intensity than the others, showing highest level of crystallization. Besides, the peak at 77.38^0 representing (311) crystalline plane is not clear in the XRD pattern of e-Ag-bio. Moreover, its lowest intensity and high noise-to-signal ratio reveal the lowest level of crystallization of e-Ag-bio, compared to the other e-AgNPs. Furthermore, the average crystallite sizes of three e-Ag samples were estimated using the Debye-Scherer's equation: $D = 0.9\lambda/(\beta \cos\theta)$. Where D is the crystallite size (nm), λ is the X-rays wavelength, β is the full width at half maximum (FWHM) intensity measured in radians, and θ is the Bragg diffraction angle of the plane. As a results, the crystallite sizes of AgNPs in e-Ag-O, e-Ag-C, e-Ag-bio samples were calculated to be 15.9, 27.3, and 16.1 nm, respectively.

3.2 e-Ag-C, e-Ag-O and e-Ag-bio nanomaterials as SERS substrates for thiram detection

To evaluate SERS sensing performance of three kinds of e-AgNPs, thiram was chosen as the analyte for SERS

measurements. Thiram solutions at different concentrations were prepared and distilled water. Fig. 2a shows SERS spectra of thiram (10^{-4} M) on e-Ag-O, e-Ag-C and e-Ag-bio. On e-Ag-O and e-Ag-C, the main characteristic bands of thiram such as 556 cm^{-1}, 928 cm^{-1}, 1150 cm^{-1} and 1382 cm^{-1} were detected. The band at 556 cm^{-1} is assigned to S–S and C–S–S stretching modes. The band at 928 cm^{-1} represents C–S stretching mode. The band at 1150 cm^{-1} is associated with N–C stretching and CH_3 rocking. The band at 1382 cm^{-1} is assigned to N–C stretching and CH_3 bending modes. In addition, the band at 1510 cm^{-1} represents C=N stretching, respectively.[20,21] It is worth noting that this double bond is not exhibit in the molecular structure of thiram (Fig. S2†). A similar double band behavior of C–N interaction of dithiocarbamate pesticides adsorbed on Au films was reported in a 2001 study, in which the authors proposed that their S–S bonds were cleaved, allowing them to chemically absorb on the metal surface *via* Au–S interactions.[20] As each thiram molecule was cleaved into two dimethyl residues, they could bind to noble metal surfaces *via* one or two S atoms, known as monodentate and bidentate interaction, respectively.[21] The double bond behavior of C–N interaction was described as a result of the formation of bidentate form. Besides, the band at 1436 cm^{-1} associated with C–N stretching is also detected in SERS spectra of thiram on e-AgNPs. It was reported to be characteristic of monodentate form.[21] The presence of these bands in the SERS spectra of thiram on e-Ag-O and e-Ag-C has confirmed the attachment of thiram on the surface of e-AgNPs *via* Ag–S interaction, forming both monodentate and bidentate. Moreover, the cleavage of S–S bond also reduced the intensity of the peak at 556 cm^{-1}. In literature, the Raman spectrum of thiram was reported, revealing that this band exhibited the highest intensity compared to other characteristic ones.[20–23] However, the SERS spectra of thiram on e-AgNPs show a peak at 556 cm^{-1} with lower intensity compared to that at 1382 cm^{-1}, which represents CH_3 bending mode. It is worth noting that CH_3 groups do not bind directly to the surface of e-AgNPs to experience the best SERS effect. Therefore, the intensity of the band at 556 cm^{-1} could have been decreased due to the S–S bond cleavage. However, this band is also associated with C–S–C stretching mode in the dimethyl residues, therefore, the band still appears in the SERS spectra of thiram.[21] Although Raman signal of thiram has been enhanced on both e-Ag-O and e-Ag-C substrates, the level of enhancement is significantly different. Fig. 2b compares SERS intensity of thiram (10^{-4} M) on e-Ag-O and e-Ag-C at several characteristic bands. On e-Ag-O, the SERS intensities of thiram (10^{-4} M) at 556 cm^{-1}, 928 cm^{-1} and 1382 cm^{-1} are around 4 time higher than those on e-Ag-C.

Concerning e-Ag-bio, several characteristic peaks of thiram were also detected in the SERS spectrum (Fig. 2a). However, the peak at 928 cm^{-1} is not detected. Instead, the peak at 881 cm^{-1} exhibits high intensity, which is different from those in SERS spectra of thiram on e-Ag-C and e-Ag-O. It is associated with $(CH_3)_2$–N and $(CH_3)_2$–N–C stretching.[21] However, it is worth noting that compounds with this structure have been detected in several plant extracts.[24] Moreover, the peak 556 cm^{-1} is shifted 20 cm^{-1} compared to the peaks detected on the other two kinds of e-AgNPs. It may be due to the complex organic coating layer of e-Ag-bio, and the peak at 928 cm^{-1} could have been overlapped by other foreign peaks. Therefore, although SERS intensities of thiram on e-Ag-bio are slightly higher than those on e-Ag-C at several characteristic peaks, it might be the result of other organic compounds in the plant extract. However, the intensity ratio between peaks at 1382 cm^{-1} and 556 cm^{-1}, which has been shifted to 536 cm^{-1}, is similar to those on e-Ag-C. Moreover, the peak at 1516 cm^{-1}, which has been shifted to 1572 cm^{-1}, could be clearly observed in the SERS spectrum of thiram on e-Ag-bio. Therefore, thiram could have

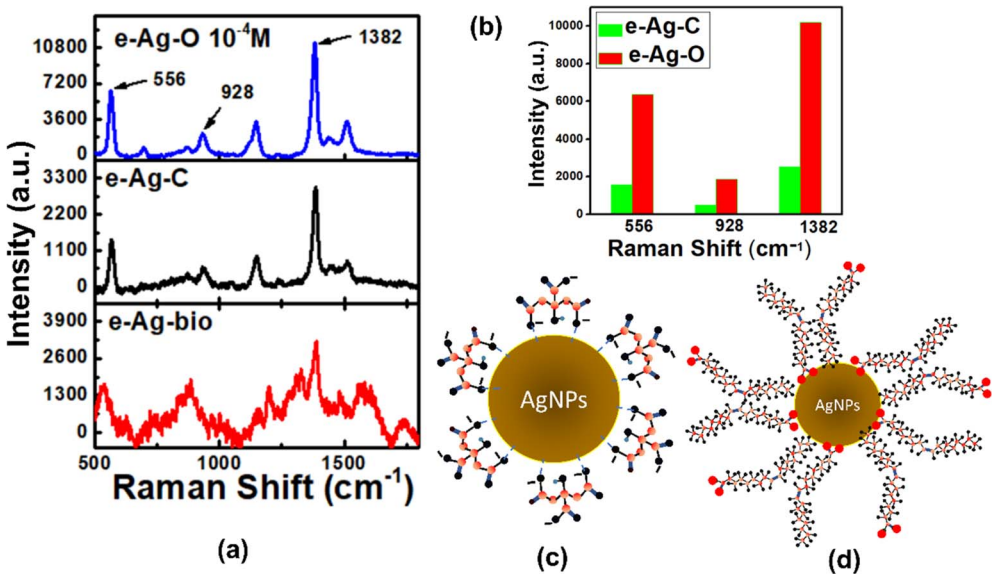

Fig. 2 (a) SERS spectra of thiram (10^{-4} M) on e-Ag-O, e-Ag-C and e-Ag-bio; (b) comparison of SERS intensities of thiram on e-Ag-C and e-Ag-O at peaks of 556, 928 and 1382 cm^{-1}; schematic structures of e-Ag-C (c) and e-Ag-O (d).

been diffused through the thick layers of e-Ag-bio to access the surface of those e-AgNPs and bind onto the Ag surface *via* Ag–S interaction. However, at a lower concentration of thiram (10^{-5} M), while SERS spectra of thiram on e-Ag-O and e-Ag-C still exhibit sharp characteristic peaks (Fig. S4†), peaks in SERS spectrum of thiram on e-Ag-bio are dull and further shifted. Therefore, it is confusing to detect them in the spectrum, preventing the determination of thiram in the sample. For that reason, e-Ag-bio is not an appropriate substrate for SERS sensing of thiram.

3.3. Effects of coating agents on SERS sensing performance of e-AgNPs

The enhancement of Raman signal of analytes on SERS substrates could be explained by both CM and EM. As discussed in Section 3.2, the adsorption of thiram on the surface of all three kinds of e-AgNPs has been reflected in the SERS spectra. Thus, it has been convenient for them to experience SERS effect *via* CM. On the other hand, the interparticle distance between nanoparticles could be observed in SEM images. To prepare for SEM measurement, e-AgNP solutions were directly drop cast on copper tape and dried in room temperature, which was similar to the preparation procedure of SERS substrates. The nature of the substrates (*i.e.*, Al and Cu) might have affect the assembly of e-AgNPs, so the distances between e-AgNPs on SERS substrate may not be completely equal. However, because the coating agents of e-AgNPs, including citrate, oleic acid and fish mint extract, are not highly reactive, so there could not be any reactions between them and the metallic surfaces (*i.e.*, Cu and Al) which seriously influence the assembly of e-AgNPs. Therefore, the behavior of e-AgNPs on SERS substrates could have been similar to that on Cu tape. As a result, the interparticle distances of e-AgNPs could be assumed to be similar to those on the SEM images: e-Ag-O < e-Ag-C < e-Ag-bio in interparticle distance. The distances of 7 nm among e-Ag-C and 4 nm among e-Ag-O are both convenient for Raman signal of thiram on those substrates to be improved *via* EM. Concerning e-Ag-bio, although the NPs were not as well distributed as the other samples with several clumps of NPs gathering, the NPs still spread over the substrate with interparticle distances ranging from 8 nm to 25 nm, allowing thiram molecules adsorbed onto those NPs to experience SERS effect in EM. Therefore, on all three kinds of e-AgNPs, SERS phenomenon could occur in both CM and EM.

To investigate the SERS enhancement through CM, we employed a UV-vis model to study the adsorption of thiram onto three kinds of e-AgNPs. In a recent study, we showed that intensity of the absorption spectra of e-AgNPs and e-AuNPs could be affected by the adsorption of analytes onto the surface of the NPs. To be detailed, the adsorption of analytes would lead to a decrease in absorption intensity of the noble metal NPs.[25] Therefore, in this study, we added 300 μL of thiram solution (10^{-5} M) into 2 mL of e-Ag-C, e-Ag-O and e-Ag-bio solutions and investigated the behavior of the adsorption peaks during incubation time. Fig. 3 shows that during the incubation time, the adsorption intensity of all three kinds of e-AgNPs decreased. However, the level of decrease and the time it took for the mixture to reach the steady state are different. To be detailed, it took only 5 min of incubation for the mixture of e-Ag-bio and thiram to reach the steady state while it required 25 and 45 min for those containing e-Ag-O and e-Ag-C, respectively. Besides, a similar trend is also observed in the decrease in intensity of the SPR peaks. At the steady state, the mixtures containing e-Ag-bio, e-Ag-O and e-Ag-C were estimated to be 90%, 95% and 82%, respectively. Accordingly, the difference in coating agent might have influenced the adsorption capacity of thiram onto the e-AgNPs. The thick coating layer of e-Ag-bio might have prevented thiram molecules from accessing the surface of the e-AgNPs. Besides, although the adsorption level of thiram onto e-Ag-O is higher than that onto e-Ag-bio, it is still much lower than that onto e-Ag-C. Different from e-Ag-bio, whose coating layers contain many kinds of phenolic acid,[26,27] the coating layers of both e-Ag-O and e-Ag-C contain single coating agents of oleic acid and citrate, respectively. In a recent study, Khutsishvili *et al.* employed XRD to confirm the covalent bonding of oxygen atoms of polar carboxylic groups of oleic acid with AgNPs.[19] Meanwhile, several other studies have been reported on the weak ionic bonding between citrate molecules and Ag surface of the nanoparticles.[28,29] Therefore, in the presence of thiram molecules, which could link to e-AgNPs *via* Ag–S covalent bonds, citrate molecules tend to be replaced while oleic acid molecules are still attached to the Ag surface. As a result, more citrate molecules could be adsorbed onto the surface of e-Ag-C even though e-Ag-O exhibits the larger surface area with a smaller size of 16 nm, compared to the larger size of 24 nm of e-Ag-C. The replacement of thiram as a coating agent onto e-Ag-C was reflected in adsorption spectra. Fig. S5† compares the SPR peak position of e-AgNP solutions before without the addition of thiram and at the steady state. Accordingly, only e-Ag-C sample shows a red-shift of 4 nm, representing the replacement of citrate on the surface of the NPs. Meanwhile, the others show no shift in adsorption peak. This investigation shows that e-Ag-C exhibits the highest level of thiram adsorption allowing the largest number of thiram molecules to experience SERS effect *via* CM. However, e-Ag-C does not show the best SERS sensing performance. It could be

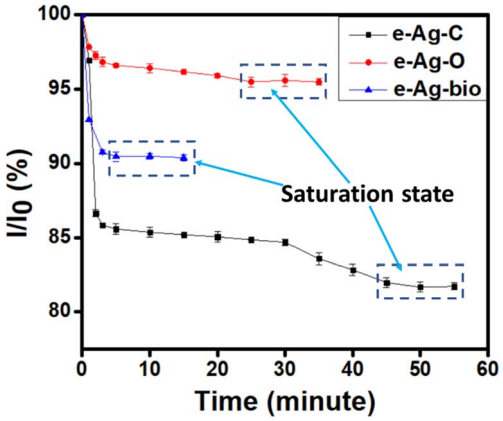

Fig. 3 Changes in absorption intensity at 410 nm for the three mixtures over the 55 min of incubation.

due to the contribution of EM enhancement in the whole SERS enhancement on these substrates.

As discussed in Section 3.1, SEM images show the self-assembly of e-Ag-C and c-Ag-O. To prepare for SEM experiments, e-AgNP solutions were drop-casted onto glass substrates and dried at room temperature, which is similar to the preparation of SERS substrates. Hence, e-Ag-C and e-Ag-O could also be self-assembled on the Al substrate with similar interparticle distances. With a smaller distance of 4 nm, e-Ag-O provide hot spots with larger EM enhancements, resulting in higher SERS intensity of thiram on e-Ag-O, compared to that on e-Ag-C. With this experimental model, we could not calculate the exact contribution of EM and CM in SERS enhancement of thiram on e-AgNPs. However, it demonstrates that EM has larger contributions to SERS enhancement than CM, which is in agreement with previous studies.[12,30]

Concerning e-Ag-bio, absorption spectra show the lowest level of thiram adsorption onto this kind of e-AgNP. Surprisingly, SERS intensity of thiram on e-Ag-bio is similar to that on e-Ag-C. In the SEM image of e-Ag-bio, although the NPs are not evenly distributed on the substrate as e-Ag-C and e-Ag-O, the interparticle distance could be estimated to be 8 nm, which promotes SERS enhancement *via* CM. In addition, compared to the other electrolytes, fish mint exact is not fully dissolved in water. The heterogeneity of the extract has prevented the formation of spherical e-AgNPs. SEM images show that e-Ag-bio is not as spherical as e-Ag-O and e-Ag-C. This morphology has a great advantage in EM enhancement, compared to the other e-AgNPs. Unfortunately, the thick coating layer has prevented thiram molecules from adsorbing onto the surface of e-Ag-bio. As a result, SERS signal of thiram on e-Ag-bio has a similar intensity compared to that on e-Ag-C.

3.4 e-Ag-O-based SERS sensors for thiram detection

With the best SERS enhancement, e-Ag-O was selected to further develop SERS sensors for thiram. Fig. 4a shows SERS spectra of thiram at seven concentrations (10^{-4} M to 10^{-10} M) on e-Ag-O. Characteristics bands of thiram could be observed in the SERS spectra of thiram at concentrations down to 10^{-9} M. At the concentration of 10^{-10} M, several characteristic peaks have disappeared. As discussed in Section 3.2, to adsorb onto Ag surface, each thiram molecule was cleaved into two dimethyl residues, which could bind to Ag surface *via* one or two S atoms, forming monodentate and bidentate interactions, respectively. Thiram residues on e-AgNPs exist in both kinds of interaction, but the equilibrium between them is different at distinct concentrations of thiram. At low concentrations, bidentate interaction predominates and *vice versa*. This transformation results in pour linear relationship between logarithmic SERS intensities at the characteristic peaks of thiram and logarithmic concentration of thiram. Fig. S6† shows plots of logarithmic SERS intensities at 928 cm^{-1} and 1382 cm^{-1} with linear regression $R^2 = 0.81$ and 0.90. It is obvious that the linear regression at 1382 cm^{-1} is higher. The band at 1382 cm^{-1} is assigned to N–C stretching and CH_3 bending modes, which are more stable than vibration modes associated with S atoms that directly involved in the binding of thiram onto Ag surface. It was reported that the predominance of monodentate or bidentate modes of thiram attached on e-AgNPs can be reflected on S-related bands.[21] For example, at the highest concentration of thiram (10^{-4} M), SERS intensity of the band at 1382 cm^{-1} is predominant (Fig. 4a), representing the predominance of bidentate form of the analyte. When the concentration of thiram increases, SERS intensity at 928 cm^{-1}, which represents C–S stretching mode, becomes nearly equal to that at 1382 cm^{-1}.

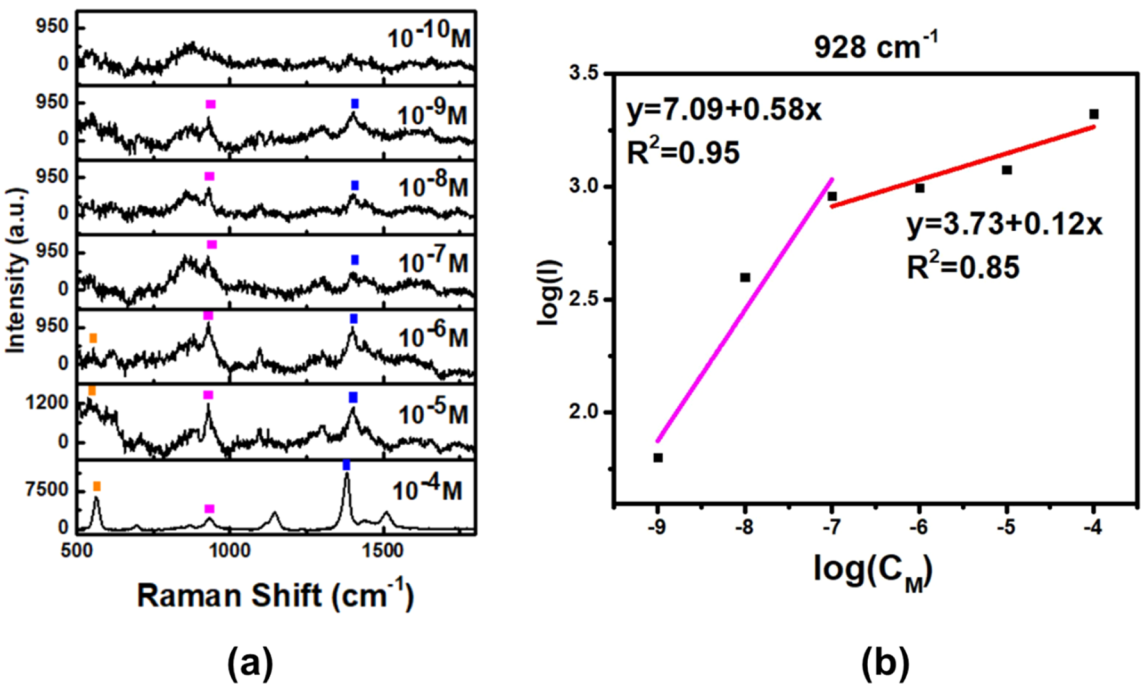

Fig. 4 (a) SERS spectra of thiram on e-Ag-O substrates and (b) linear response at 928 cm^{-1} of thiram at different concentrations.

Table 1 Reported SERS sensors for thiram detection

NPs	LOD	Linear range	Repeata-bility	Reprodu-cibility	Real sample	Ref
Ag nanocube	10^{-14} M	—	10.54%	—	—	5
Ag nanowire	10^{-9} M	—	14.06%	—	—	
Ag dendrite	10^{-7} M (in grape juice)	10^{-7} to 10^{-4} M (in grape juice)	—	—	Grape juice	31
Au nanostar	10^{-10} M (in standard samples) 10^{-7} M (in apple juice)	—	—	—	Apple peel	32
e-AuNPs (citrate coated)	5×10^{-10} M	—	17%	10.5%	—	25
e-Ag-O	1.04×10^{-10} M	10^{-9} to 10^{-7} M 10^{-7} to 10^{-4} M	13.8%	6.89%	Tea leaves	This work

It could be explained by the formation and predominance of monodentate mode of thiram. However, the band at 928 cm^{-1} does not exhibit higher intensity than that at 1382 cm^{-1} because of the remarkably strong intensity of the methyl groups described by Sánchez-Cortés *et al.*[20] The intensity at 928 cm^{-1} keeps increasing with the increase of thiram concentration forming two linear plots of logarithmic SERS intensity at 928 cm^{-1} against logarithmic concentration of thiram at low concentrations (10^{-9} M to 10^{-7} M) and high concentrations (10^{-7} M to 10^{-4} M). It could be due to the predominence of bidentate at low concentrations and monodentate at low concentrations of thiram. Based on the linear equation at low concentrations of thiram shown in Fig. 4b, LOD was calculated to be 1.04×10^{-10} M, which is lower than many reported noble metal-based SERS sensors for thiram (Table 1). This LOD is still higher than those when using Ag nanocubes and Au nanostars, which could generate enormous EM enhancements thanks to their hot spot formation. Instead, e-Ag-O could be fabricated using a fast, simple and eco-friendly procedure. Besides, the reproducibility of the method was evaluated by measuring SERS signal of thiram (10^{-4} M) on 5 e-Ag-O/Al substrates, which were prepared independently (Fig. 5a), resulting in a relative standard deviation (RSD) of 6.89% good reproducibility of the method. In addition, thanks to the purity of e-AgNPs, they were spread quite evenly on the Al substrate, reflected in similar SERS signal of thiram at five different positions on a substrate (Fig. 5b). The RSD was calculated to be 13.8%. LOD and RSD values were calculated as described in ESI.†

3.5 Practicability of e-Ag-O-based SERS sensors for thiram detection in real samples of green tea leaves

The practicability of e-Ag-O-based SERS sensor for thiram was investigated by detecting thiram in real tea samples collected from Thai Nguyen province, Vietnam. Thiram at six concentrations were prepared in tea samples as described in Section 2.3. Fig. 6 displays Raman spectra of thiram (10^{-4} M to 10^{-9} M) in tea samples on e-Ag-O. The characteristic peaks at 556 cm^{-1}, 928 cm^{-1} and 1382 cm^{-1} could be detected in the spectra, confirming the presence of thiram in the real samples. Although the presence of organic compounds in tea exact has increased noise-to-signal ratio in the SERS spectra, the specific Ag–S bond between thiram and e-Ag-O allowed this pesticide to be detected at concentrations down to 10^{-9} M. Using two equations in Fig. 4b, concentrations of thiram in real samples were calculated (Table 2). For the sample of 10^{-7} M, the calculated concentration of thiram is the mean of the concentrations estimated using both equations. Recovery rates range from 93% to 132%, reflecting high accuracy of the sensing system. This

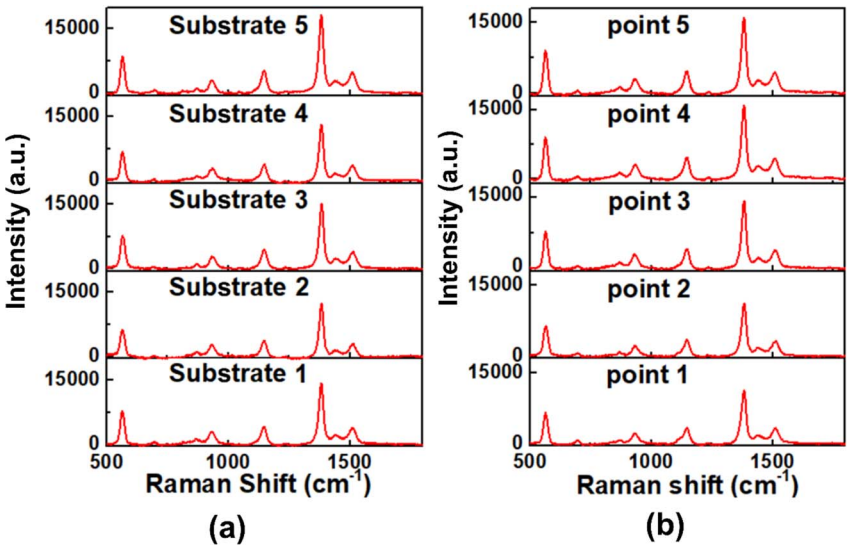

Fig. 5 Reproducibility (a) and stability (b) of SERS sensor for thiram (10^{-4} M) detection based on e-Ag-O substrates.

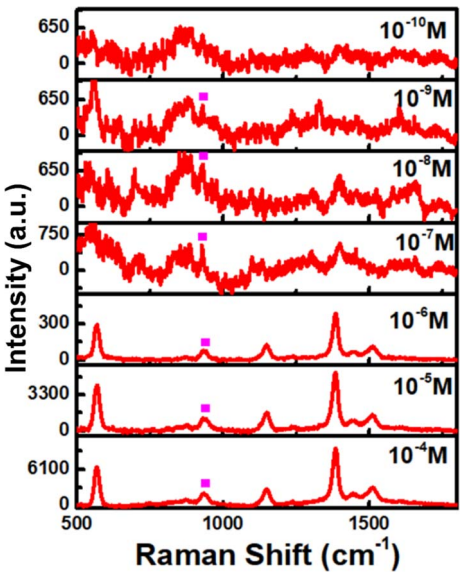

Fig. 6 SERS spectra of thiram in real samples of green tea leaves at different concentrations.

Table 2 Practicability of e-Ag-O-based SERS sensor for thiram detection in green tea leaves

Spike concentration of thiram (M)	Calculated concentration of thiram (M)	Recovery (%)
10^{-4}	3.23×10^{-5}	112
10^{-5}	2.46×10^{-7}	132
10^{-6}	2.09×10^{-7}	111
10^{-7}	5.23×10^{-8}	113
10^{-8}	2.6×10^{-8}	95
10^{-9}	3.67×10^{-9}	93

linear range covers the maximum residue levels (MRLs) for plant commodities of 2–13 ppm (7.7×10^{-6} M to 5×10^{-5} M) established by the United States Environment Protection Agency and European Food Safety Authority.

4. Conclusions

In this study, we fabricated three kinds of AgNPs using electrochemical method with the use of three different electrolytes, including citrate (e-Ag-C), oleic acid (e-Ag-O) and fish mint extract (e-Ag-bio). All as-prepared e-AgNPs exhibit SERS effect with the ability to enhance Raman signal of thiram. However, e-Ag-O shows the best SERS sensing performance. Although the level of thiram adsorption onto e-Ag-O is not as high as that onto e-Ag-C, the advantage of smallest interparticle distance allows it to generate SERS effect through electromagnetic mechanism, leading to the best improvement in Raman signal of thiram. e-Ag-O was then employed as an active SERS substrate for thiram detection with large linear ranges from 10^{-4} M to 10^{-7} M and from 10^{-7} M to 10^{-9} and an impressive LOD of 1.04×10^{-10} M. This sensor could also detect thiram in tea leaves at the concentrations down to 10^{-9} M, with the same linear ranges, which cover the MRLs for plant commodities established by the United States Environment Protection Agency and European Food Safety Authority (2–13 ppm ~7.7×10^{-6} M to 5×10^{-5} M).

Author contributions

D. T. Linh: methodology, validation, investigation, writing – original draft; Q. D. Mai: conceptualization, validation, investigation, writing – review & editing; D. T. N. Nga: conceptualization, validation, investigation, N. T. Anh: validation, investigation, writing – review & editing; H. V. Tuan: validation, investigation, methodology; H. A. Nguyen: conceptualization, methodology, formal analysis, writing – review & editing; V. X. Hoa: methodology, investigation, supervision; A. T. Le: conceptualization, methodology, supervision, project administration, writing – review & editing.

Conflicts of interest

The authors declare that they have no known competing financial interests or personal relationships that could have appeared to influence the work reported in this paper.

Acknowledgements

This research was supported by the Phenikaa University under grant number PU2023-2-A-03 and was also acknowledged to the Phenikaa Group through Financial Supports for Key Research Group (NEB Lab). The authors would like to acknowledge the supports for Raman & UV-vis measurements from NEB Lab (Phenikaa University), XRD measurements from VNU-Hanoi and SEM characterization from GUST-VAST.

References

1 H. M. Lee, S. M. Jin, H. M. Kim and Y. D. Suh, Single-molecule surface-enhanced Raman spectroscopy: a perspective on the current status, *Phys. Chem. Chem. Phys.*, 2013, **15**, 5276–5287.
2 A. I. Pérez-Jiménez, D. Lyu, Z. Lu, G. Liu and B. Ren, Surface-enhanced Raman spectroscopy: benefits, trade-offs and future developments, *Chem. Sci.*, 2020, **11**, 4563–4577.
3 R. Pilot, R. Signorini, C. Durante, L. Orian, M. Bhamidipati and L. Fabris, A review on surface-enhanced Raman scattering, *Biosensors*, 2019, **9**, 5.
4 E. Petryayeva and U. J. Krull, Localized surface plasmon resonance: nanostructures, bioassays and biosensing—A review, *Anal. Chim. Acta*, 2011, **706**, 8–24.
5 M. B. Bhavya, B. M. Shenoy, P. Bhol, S. Swain, M. Saxena, N. S. John, G. Hegde and A. K. Samal, Femtomolar detection of thiram via SERS using silver nanocubes as an efficient substrate, *Environ. Sci.: Nano*, 2020, **7**, 3999–4009.
6 N. H. Anh, M. Q. Doan, N. X. Dinh, T. Q. Huy, D. Q. Tri, B. Van Hao and A.-T. Le, Gold nanoparticle-based optical nanosensors for food and health safety monitoring: recent advances and future perspectives, *RSC Adv.*, 2022, **12**, 10950–10988.

7 N. T. Anh, N. X. Dinh, H. Van Tuan, M. Q. Doan, N. H. Anh, N. T. Khi, V. T. Trang, D. Q. Tri and A.-T. Le, Eco-friendly copper nanomaterials-based dual-mode optical nanosensors for ultrasensitive trace determination of amoxicillin antibiotics residue in tap water samples, *Mater. Res. Bull.*, 2022, **147**, 111649.
8 A. M. Ondieki, Z. Birech, K. A. Kaduki, P. W. Mwangi, N. M. Mwenze, M. Juma, C. Jeptoo, M. S. Dlamini and M. Maaza, Fabrication of surface-enhanced Raman spectroscopy substrates using silver nanoparticles produced by laser ablation in liquids, *Spectrochim. Acta, Part A*, 2023, 122694.
9 J. Lu, Z. Cai, Y. Zou, D. Wu, A. Wang, J. Chang, F. Wang, Z. Tian and G. Liu, Silver nanoparticle-based surface-enhanced Raman spectroscopy for the rapid and selective detection of trace tropane alkaloids in food, *ACS Appl. Nano Mater.*, 2019, **2**, 6592–6601.
10 A. Rajput, S. Kumar and J. P. Singh, Vertically standing nanoporous Al–Ag zig-zag silver nanorod arrays for highly active SERS substrates, *Analyst*, 2017, **142**, 3959–3966.
11 S. K. Gahlaut, A. Pathak and B. D. Gupta, Recent advances in silver nanostructured substrates for plasmonic sensors, *Biosensors*, 2022, **12**, 713.
12 Y.-T. Chen, L. Pan, A. Horneber, M. van den Berg, P. Miao, P. Xu, P.-M. Adam, A. J. Meixner and D. Zhang, Charge transfer and electromagnetic enhancement processes revealed in the SERS and TERS of a CoPc thin film, *Nanophotonics*, 2019, **8**, 1533–1546.
13 Z. Chen, T. Balankura, K. A. Fichthorn and R. M. Rioux, Revisiting the polyol synthesis of silver nanostructures: role of chloride in nanocube formation, *ACS Nano*, 2019, **13**, 1849–1860.
14 F.-Z. Cong, H. Wei, X.-R. Tian and H.-X. Xu, A facile synthesis of branched silver nanowire structures and its applications in surface-enhanced Raman scattering, *Front. Phys.*, 2012, **7**, 521–526.
15 Y. Qu, C. Tan, Z. Zhang and L. He, A facile solvent mediated self-assembly silver nanoparticle mirror substrate for quantitatively improved surface enhanced Raman scattering, *Analyst*, 2017, **142**, 4075–4082.
16 H. Jason and S. Konstantin, Synthesis of stable citrate-capped silver nanoprisms, *Langmuir*, 2017, **33**, 10525–10530.
17 E. de Barros Santos, N. V. Madalossi, F. A. Sigoli and I. O. Mazali, Silver nanoparticles: green synthesis, self-assembled nanostructures and their application as SERS substrates, *New J. Chem.*, 2015, **39**, 2839–2846.
18 M. Q. Doan, N. H. Anh, N. X. Quang, N. X. Dinh, D. Q. Tri, T. Q. Huy and A.-T. Le, Ultrasensitive detection of methylene blue using an electrochemically synthesized SERS sensor based on gold and silver nanoparticles: roles of composition and purity on sensing performance and reliability, *J. Electron. Mater.*, 2022, **51**, 150–162.
19 S. S. Khutsishvili, P. Toidze, M. Donadze, M. Gabrichidze, N. Makhaldiani and T. Agladze, Structural surface features of paramagnetic multifunctional nanohybrids based on silver oleic acid, *J. Cluster Sci.*, 2021, **32**, 1351–1359.
20 S. Sánchez-Cortés, C. Domingo, J. V. García-Ramos and J. A. Aznárez, Surface-enhanced vibrational study (SEIR and SERS) of dithiocarbamate pesticides on gold films, *Langmuir*, 2001, **17**, 1157–1162.
21 M. J. S. Oliveira, C. S. Martin, R. J. G. Rubira, A. Batagin-Neto, C. J. L. Constantino and R. F. Aroca, Surface-enhanced Raman scattering of thiram: quantitative and theoretical analyses, *J. Raman Spectrosc.*, 2021, **52**, 2557–2571.
22 M. Chen, W. Luo, Q. Liu, N. Hao, Y. Zhu, M. Liu, L. Wang, H. Yang and X. Chen, Simultaneous in Situ Extraction and Fabrication of Surface-Enhanced Raman Scattering Substrate for Reliable Detection of Thiram Residue, *Anal. Chem.*, 2018, **90**, 13647–13654.
23 J. Zhu, Q. Chen, F. Y. H. Kutsanedzie, M. Yang, Q. Ouyang and H. Jiang, Highly sensitive and label-free determination of thiram residue using surface-enhanced Raman spectroscopy (SERS) coupled with paper-based microfluidics, *Anal. Methods*, 2017, **9**, 6186–6193.
24 T. V. T. Do, W. Suhartini, C. U. Phan, Z. Zhang, G. Goksen and J. M. Lorenzo, Nutritional value, phytochemistry, health benefits, and potential food applications of Pouteria campechiana (Kunth) Baehni: a comprehensive review, *J. Funct. Foods*, 2023, **103**, 105481.
25 N. H. Anh, M. Q. Doan, N. X. Dinh, T. Q. Huy, D. Q. Tri and A.-T. Le, Gold nanoparticles-based SERS nanosensor for thiram and chloramphenicol monitoring in food samples: insight into effects of analyte molecular structure on their sensing performance and signal enhancement, *Appl. Surf. Sci.*, 2022, **584**, 152555.
26 Z. Wu, X. Deng, Q. Hu, X. Xiao, J. Jiang, X. Ma and M. Wu, Houttuynia cordata thunb: an ethnopharmacological review, *Front. Pharmacol*, 2021, **12**, 714694.
27 W. Cai, Y. Xu, J. Shao, S. Dai, Q. Liu, Z. Liu and W. Wu, Phenolic contents and antioxidant activities of different parts of Houttuynia cordata Thunb, *J. Med. Plants Res.*, 2012, **6**, 1035–1040.
28 P. Wulandari, T. Nagahiro, N. Fukada, Y. Kimura, M. Niwano and K. Tamada, Characterization of citrates on gold and silver nanoparticles, *J. Colloid Interface Sci.*, 2015, **438**, 244–248.
29 Y.-M. Long, L.-G. Hu, X.-T. Yan, X.-C. Zhao, Q.-F. Zhou, Y. Cai and G.-B. Jiang, Surface ligand controls silver ion release of nanosilver and its antibacterial activity against Escherichia coli, *Int. J. Nanomed.*, 2017, 3193–3206.
30 H. K. Lee, Y. H. Lee, C. S. L. Koh, G. C. Phan-Quang, X. Han, C. L. Lay, H. Y. F. Sim, Y.-C. Kao, Q. An and X. Y. Ling, Designing surface-enhanced Raman scattering (SERS) platforms beyond hotspot engineering: emerging opportunities in analyte manipulations and hybrid materials, *Chem. Soc. Rev.*, 2019, **48**, 731–756.
31 Q. Wang, D. Wu and Z. Chen, Ag dendritic nanostructures for rapid detection of thiram based on surface-enhanced Raman scattering, *RSC Adv.*, 2015, **5**, 70553–70557.
32 J. Zhu, M.-J. Liu, J.-J. Li, X. Li and J.-W. Zhao, Multi-branched gold nanostars with fractal structure for SERS detection of the pesticide thiram, *Spectrochim. Acta, Part A*, 2018, **189**, 586–593.